Combinations of muscle synergies in the construction of a natural motor behavior

Andrea d'Avella[1,2], Philippe Saltiel[1] and Emilio Bizzi[1]

[1] *Department of Brain and Cognitive Sciences and McGovern Institute for Brain Research, Massachusetts Institute of Technology, 45 Carleton St., Cambridge, Massachusetts 02139, USA*

[2] *Human Physiology Section, IRCCS Fondazione Santa Lucia, Via Ardeatina 306, 00179 Rome, Italy*

Correspondence should be addressed to E.B. (ebizzi@mit.edu)

Published online 3 February 2003; doi:10.1038/nn1010

A central issue in motor control is how the central nervous system generates the muscle activity patterns necessary to achieve a variety of behavioral goals. The many degrees of freedom of the musculoskeletal apparatus provide great flexibility but make the control problem extremely complex. Muscle synergies—coherent activations, in space or time, of a group of muscles—have been proposed as building blocks that could simplify the construction of motor behaviors. To evaluate this hypothesis, we developed a new method to extract invariant spatiotemporal components from the simultaneous recordings of the activity of many muscles. We used this technique to analyze the muscle patterns of intact and unrestrained frogs during kicking, a natural defensive behavior. Here we show that combinations of three time-varying muscle synergies underlie the variety of muscle patterns required to kick in different directions, that the recruitment of these synergies is related to movement kinematics, and that there are similarities among the synergies extracted from different behaviors.

A key question in the study of neural control of limb movement is how the CNS coordinates the large number of degrees of freedom of the musculoskeletal system and overcomes the complexity of limb dynamics to achieve a variety of behavioral goals[1]. In many circumstances, the CNS cannot rely on sensory feedback[2], but must use an open-loop control law to generate appropriate muscle patterns. Implementing such a controller, however, presents a great computational challenge because it requires mapping a potentially infinite number of different goals onto an infinite set of muscle patterns. An efficient solution might be achieved by representing all useful muscle patterns as combinations of a small number of generators. This would reduce the dimensionality of the problem and allow sharing of neural circuitry across many tasks. Indeed, the idea that the CNS might simplify the control problem by combining discrete elements is a long-standing one in motor neurophysiology. Reflexes[3], unit burst generators[4], spinal force fields[5–7] and muscle synergies[8,9] have each been proposed as possible building blocks. The challenge, however, has been to establish the existence of these conjectured building blocks and their role in the construction of natural motor behaviors. Specifically, most of the evidence for discrete elements derives from experiments with spinalized or decerebrated preparations. The behavior of these preparations lacks the complexity and variability typical of an intact animal interacting with an environment to achieve meaningful behavioral goals.

Here we address this limitation directly by examining a natural behavior of intact, freely moving animals. We characterized the organization of the controller by identifying features in the motor output that were invariant across the entire repertoire of movements of a natural motor behavior. In particular, we investigated the existence of a small set of muscle synergies[10,11] as generators for the entire set of muscle patterns. We tested a specific model for the construction of muscle patterns from muscle synergies, and from our findings, we propose that the fundamental building blocks are time-varying muscle synergies (coordinated activations of groups of muscles with specific time-varying profiles). An individual time-varying muscle synergy can be thought of as a fixed motor program. Extending this idea, we further propose that muscle patterns are constructed by combinations of time-varying synergies that are independently scaled in amplitude and shifted in time. The simultaneous and independent recruitment of different synergies provides the flexibility necessary to capture the variability of the muscle patterns involved in a natural behavior. As it imposes specific spatiotemporal profiles on the generators and thus explicitly predicts the temporal structure of the muscle patterns, this model differs from other recently proposed synergy combination models[8,9].

To identify a set of time-varying muscle synergies from the entire set of muscle patterns recorded during defensive kicking, we developed a new decomposition algorithm[12]. Here we show that a large fraction of the variation in the muscle activity patterns used for kicks in different directions is described by combinations of three time-varying muscle synergies. Moreover, the recruitment of two of these synergies is modulated across different kicks, and these modulations reflect systematic changes in the kick kinematics. These results suggest that a small set of discrete elements underlie the generation of a variety of behaviorally significant movements.

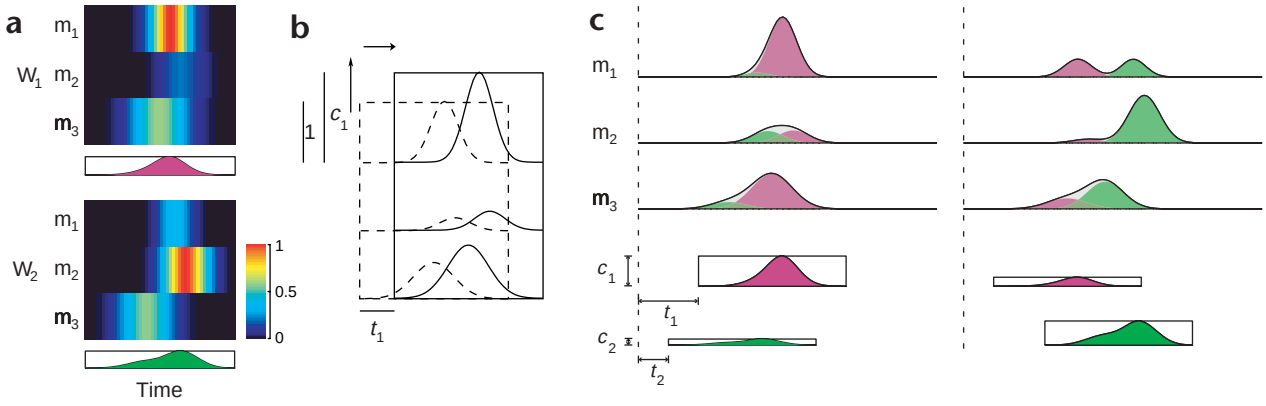

Fig. 1. Time-varying synergies model. In this simulated example, two time-varying synergies (**a**) are scaled in amplitude and shifted in time (**b**), and then combined to construct two different patterns (**c**). (**a**) The rows in each synergy (W_1 and W_2) represent the activation time courses of the three muscles (m_1 to m_3), with the amplitude, shown in color code, normalized within each synergy to the value of the maximum sample. The profile in the box below each synergy represents the time course of the synergy averaged across muscles. (**b**) To generate a specific muscle pattern, every muscle in each synergy is first scaled in amplitude by a non-negative coefficient (c_1 in the illustration representing the time course of the three muscles of W_1) and shifted in time by an onset delay (t_1). The three curves in a box represent W_1 before (dashed traces) and after (solid traces) scaling and shifting. (**c**) The elements of the first synergy (magenta shaded area) are then summed together with corresponding elements of the second synergy (green shaded area) to generate the complete pattern (solid line). In this illustration, the amplitude coefficients (c_1 and c_2) are represented as the height of the rectangles below the muscle patterns, and the onset delays (t_1 and t_2) are represented by the horizontal position of the left edge of the rectangle.

Results

Time-varying synergies model

We modeled the generation of muscle patterns as linear combinations of time-varying synergies, that is, time-varying profiles of muscle activity, that were recruited with variable intensity and with variable onset time. To illustrate the model, we show a sample reconstruction of two different patterns that involve three muscles as combinations of two simulated time-varying synergies (**Fig. 1**). Each synergy (W_1 and W_2 in **Fig. 1a**) represents the time course of the activation level for the three muscles (m_1 to m_3). To generate specific muscle patterns (**Fig. 1c**), each synergy is first scaled in amplitude by a non-negative coefficient (c_1 and c_2) and shifted in time by an onset delay (t_1 and t_2), and then the elements corresponding to the same muscle and time sample in different synergies are summed together (Methods). Given one set of synergies, a variety of different patterns can be generated by choosing different amplitude and delay coefficients.

Synergies in frog kicking

We tested this model on a large set of muscle patterns recorded simultaneously from 13 hindlimb muscles in four frogs during kicking. After cutaneous stimulation of the foot, we observed a fast extension of one limb with the other limbs and the body stationary and a flexion repositioning the limb in a crouched resting posture. At the point of maximum extension, the ankle reached different positions—medial, caudal or lateral to the starting position.

We extracted a single set of time-varying synergies from the entire set of electromyographic (EMG) patterns from 239 kicks

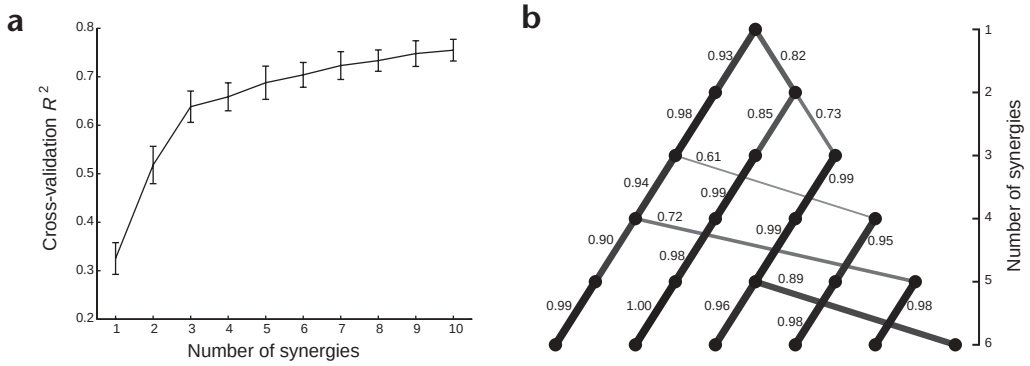

Fig. 2. Selection of the number of synergies. (**a**) Cross-validation procedure. For each number of synergies, the extraction is performed on a randomly selected 80% of the data, and the reconstruction tested on the remaining 20% of the data. Mean and standard deviation of the fraction of total variation (R^2) of five disjoint test sets explained by the synergies extracted from the remaining data is shown. The slope of the curve changes sharply at three, indicating that four or more synergies capture only a small additional fraction of the total variation in the data explained by three synergies. (**b**) Similarities between sets with different numbers of synergies. The nodes on each row of the pyramid represent the synergies extracted from sets with a number of elements ranging from 1 to 6. The links between the nodes in two adjacent rows connect synergies that are similar (similarity value above 0.6, with the value computed as the maximum of the normalized scalar product at different delays; Methods). The degree of similarity is indicated by the thickness and darkness of the link and the value shown close to each link.

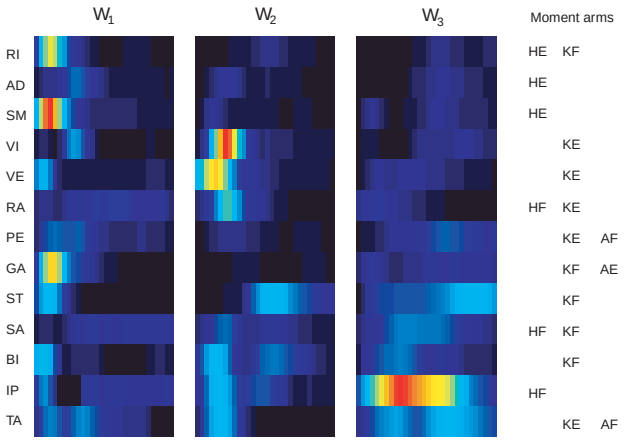

Fig. 3. Three time-varying synergies extracted from the entire kicking dataset. The first three columns (W_1 to W_3) represent the three extracted synergies as color-coded (same scale as in **Fig. 1**) activation time course of 13 muscles over 30 samples (300 ms total duration) normalized to the maximum sample. The three synergies capture different features of the kicking muscle patterns: W_1 and W_2 show an high level of activation, especially in extensor muscles (in particular the hip extensor RI and SM for the first synergy and the knee extensor VI and VE for the second). Mostly flexor muscles (IP, ST, TA, SA, BI) are recruited in W_3. The fourth column indicates the sign (flexion or extension) of the moment arms around hip, knee and ankle joints of the 13 muscles included in each synergy (HE: hip extension; HF: hip flexion; KE: knee extension; KF: knee flexion; AE: ankle extension; AF: ankle flexion).

using a decomposition procedure based on an optimization algorithm[12]. Starting from random initial conditions, the algorithm finds a set of synergies and coefficients that minimize the total reconstruction error by iterating three different steps (Methods).

We selected the number of synergies according to two criteria. First, we used a cross-validation procedure[13] to determine at which point the model begins to fit statistical fluctuations more than capturing structure in the data. We computed the fraction of total variation (R^2) explained in 20% of the data by the synergies extracted from the remaining 80% of the data as a function of the number of synergies (**Fig. 2a**). This curve has a sharp change in slope at three synergies, indicating that sets with four or more synergies explain only a small additional fraction of total variation in the data captured with three synergies. Second, we compared sets with increasing number of extracted synergies to assess whether adding a synergy induces changes in the entire set (**Fig. 2b**). This graph shows which pairs of synergies had a similarity above 0.6 (Methods). The nodes in the graph are connected by diagonals made of high-similarity links, indicating that all the synergies extracted from a set with N synergies are essentially preserved in the set with $N + 1$ synergies. This fact ensures that the analysis performed choosing a particular set will be consistent with the analysis based on larger sets. Therefore, considering the cross-validation R^2 curve, we chose three synergies.

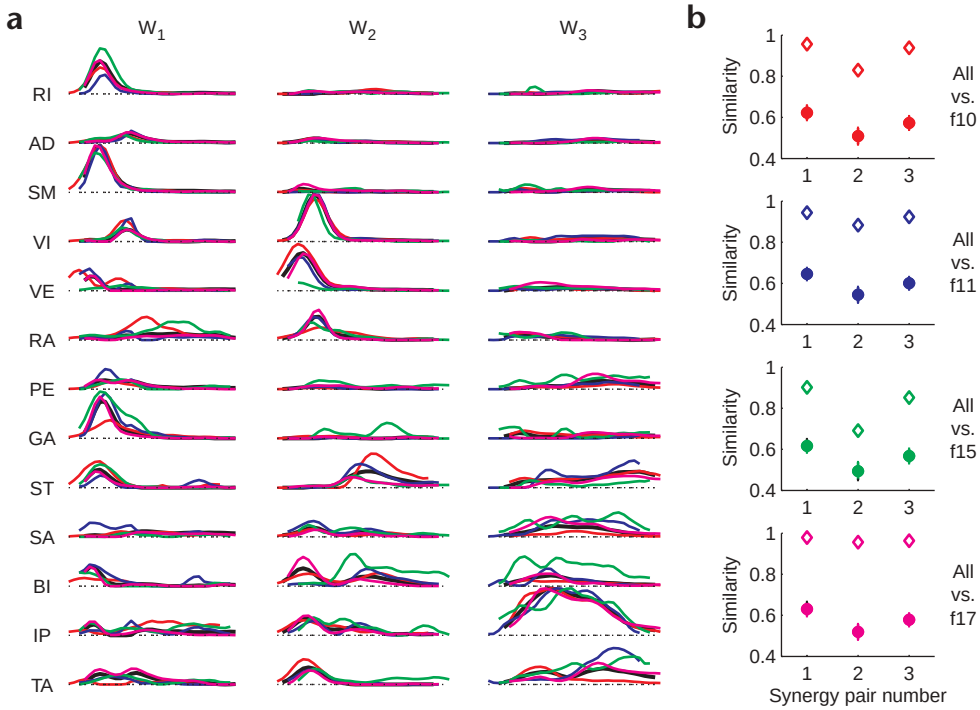

Fig. 4. Synergies extracted from individual animals. (**a**) Comparison between the three synergies extracted using the data pooled from four frogs (black trace, same synergies of **Fig. 3**), with the synergies extracted from individual frogs (red trace, f10, n = 86; blue trace, f11, n = 33; green trace, f15, n = 18; magenta trace, f17, n = 102). Each synergy extracted from an individual frog is grouped and aligned with the most similar synergy in the set extracted from the pooled data. (**b**) Similarities between synergies from pooled and individual frogs. Each one of the four plots shows the similarities between the three synergies extracted from pooled data with the best matching synergies extracted from one frog (open diamonds) and the similarities between the best matching pairs of random synergies (filled circles, mean ± s.d.) out of two sets generated according to the amplitude distributions of the two corresponding datasets (Methods).

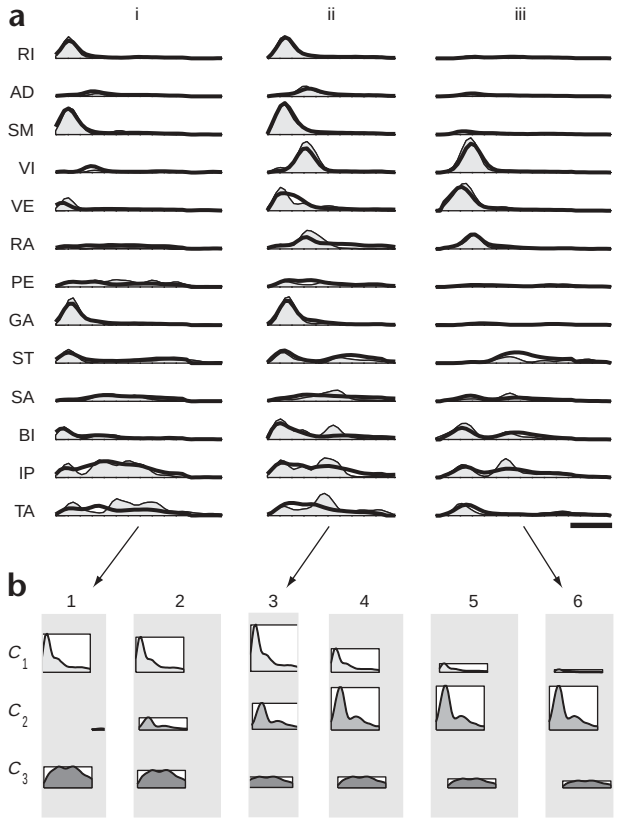

Fig. 5. Reconstruction of kick muscle patterns as combinations of time-varying synergies. (**a**) Three different patterns (rectified, filtered and integrated EMGs, i to iii, thin line and shaded area) are reconstructed by scaling in amplitude, shifting in time, and summing together the three synergies extracted from pooled data (thick line). Scale bar, 100 ms. (**b**) The amplitude coefficients (c_1 to c_3) for the three kicks in (**a**) (1, 3 and 6) and three other kicks are illustrated as the height of three rectangles, whereas the horizontal position of the rectangles represents the position in time of the synergies with respect to the extent of the muscle pattern (gray background). The profiles within each rectangle represent the time-course of the synergies averaged over the 13 muscles. The three examples in (**a**) show how the first two synergies are independently combined to generate different kicks: the first synergy and not the second is recruited for a medially directed kick (i and 1), involving mainly hip extension; the second synergy and not the first is recruited for a lateral kick (iii and 6), obtained with a knee extension; a caudal kick (ii and 3), involving both a knee and a hip extension, is constructed by a combination of the two synergies. A systematic modulation of amplitude and timing of the recruitment of the first two synergies can be seen in the six examples shown in (**b**).

The R^2 for the three synergies extracted from the entire dataset was 0.65. Thus, a large fraction of the total variation of the data was described by a model that, once the synergies are determined, has just six parameters (three amplitudes and three timing coefficients) for each kick. In comparison, the reconstruction of the same dataset with three randomly generated time-varying synergies (Methods) was much poorer ($R^2 = 0.19 \pm 0.02$).

The three extracted synergies (**Fig. 3**) include by definition all 13 muscles and comprise 30 samples, corresponding to 300 ms of electromyogram (EMG) recording. The first two synergies (W_1 and W_2 in **Fig. 3**) represent short bursts of various, mainly extensor, muscles. The third synergy (W_3) describes instead longer bursts involving mainly flexor muscles. The muscle composition and the temporal structure of these synergies suggest a functional specificity: the first two synergies appear to be responsible for the faster extension phase of the kicks and the third synergy for the flexion phase. Of the two extension synergies, the first involves mainly hip extensor muscles and the second mainly knee extensors.

Comparison across animals

The synergies described above were extracted using the data pooled from four frogs. We next tested whether the same synergies were consistently extracted from individual animals. The synergies extracted from each individual frog (**Fig. 4a**, colored lines) are generally very similar to each other and to the synergies extracted from the pooled data (**Fig. 4a**, black line, same synergies as in **Fig. 3**), with the exception of one frog (green line) whose synergies were extracted from the smallest of the four data sets. The degree of similarity between the synergies extracted from the pooled data and the synergies extracted from the individual frogs (open diamonds in **Fig. 4b**) is much higher than the degree of similarity between randomly generated synergies (filled circles in **Fig. 4b** and Methods), confirming the above qualitative observation of highly consistent synergies across animals.

Reconstruction of muscle patterns

In three representative examples, the essential features of the observed EMG patterns (**Fig. 5a**, thin line and shaded area) are well reconstructed by scaling in amplitude and shifting in time the three time-varying synergies (**Fig. 5a**, thick line). The first pattern (left column i), recorded during a medially directed kick involving hip extension and some knee flexion, is constructed by combining the first and the third synergy (**Fig. 5b**, column 1). The second synergy is not recruited for this kick. In contrast, the third pattern (**Fig. 5a**, right column iii), producing a lateral kick consisting of a knee extension, is constructed by the combination of the second and third synergies with a minimal contribution from the first synergy (**Fig. 5b**, column 6). These two examples suggest that the first two synergies can be independently added to the third synergy to generate different patterns. The second example (**Fig. 5a**, middle column ii), a pattern observed in a caudally directed kick involving hip and knee extension, shows that the recruitment of the first two synergies is not exclusive, but they can be activated together (**Fig. 5b**, column 3).

A gradual transition from a pattern with only the first and third synergies to one with only the second and third synergies can be seen considering additional examples (**Fig. 5b**). In addition to a clear modulation of the synergy amplitudes, these examples also show a modulation of the synergy onset times, shifting from an onset of the first synergy before the second synergy (columns 1 to 3) to an onset of the second synergy before the first synergy (columns 5 and 6). Moreover, the consideration of the direction of these kicks suggests a functional significance for this modulation of the recruitment of the two extension synergies: the kick direction shifts from medial (hip extension) to caudal (hip and knee extension) to lateral (knee extension) as we progress from the first to the last example.

Synergy recruitment and kick kinematics

To investigate the functional role of the two extension synergies, we studied systematically the relationship between their recruitment and the kick kinematics. We measured the joint angles from digitized video frames and characterized the kick kinematics with a vector representing the displacement in the hip–knee plane from the initial limb position to the end of the extension phase. Both

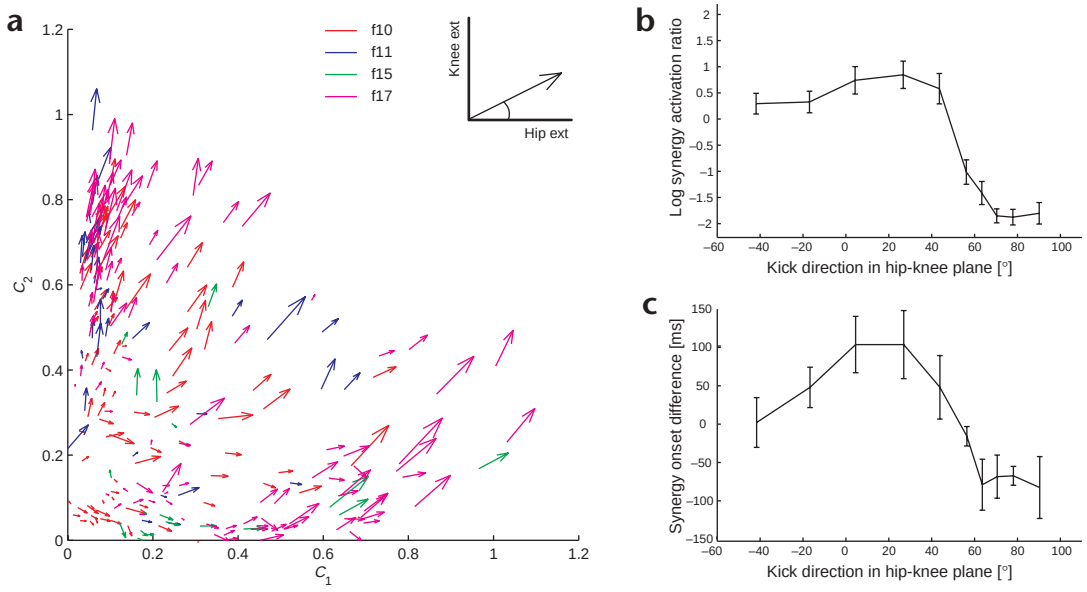

Fig. 6. Relationship between kick kinematics and recruitment of two synergies. (**a**) Relationship between kick kinematics and synergy activation coefficients. The displacement vector in the hip-knee plane from initial position to maximum extension is represented as an arrow for each of the 239 kicks recorded in four frogs. The coordinates of the arrow's tail indicate the amplitude coefficients (c_1 and c_2) of the first two synergies (W_1 and W_2 in **Fig. 3**) used in the reconstruction of each kick. (**b**, **c**) Dependence of synergy recruitment on kick direction. The logarithm of the ratio of c_1 over c_2 (**b**) and the difference of the onset time (**c**) between the second and the first synergies ($t_2 - t_1$) for kicks with c_1 and c_2 above their 10% percentile (n = 191) is averaged (mean ± s.e.m.) in ten bins of the angle of kick direction in the hip–knee plane with respect to the pure hip extension direction (0°; a pure knee extension corresponds to a 90° angle).

the direction and the magnitude of the displacement vectors depend on the level of activation of the two synergies (**Fig. 6a**). In particular, the direction of the displacement vector and hence the direction of limb movement depends on the relative amount of the synergy activation coefficients (c_1 and c_2). To quantify this, we computed the average of the logarithm of the two activation coefficients over ten bins of the displacement vector direction (**Fig. 6b**). Kicks characterized by hip extension with some knee flexion or knee extension (first five bins in **Fig. 6b**) have on average $c_1 > c_2$ (positive logarithm). When the amount of knee extension is increased, the ratio shifts (bins six and seven) toward the opposite balance of synergy activation. Kicks with mainly knee extension (last three bins) have a much larger c_2 than c_1 (negative logarithm).

We also studied the relationship between kick kinematics and temporal recruitment of the two extension synergies. As suggested by the examples above (**Fig. 5b**), we observed a systematic shift of the difference in the synergy activation delay with changes in kick direction. The average delay difference over ten bins of the displacement vector direction shifts from positive (W_2 after W_1) for kicks with large hip extension to negative (W_2 before W_1) for kicks with large knee extension (**Fig. 6c**).

Comparison with other behaviors

We next investigated whether the synergies extracted from kicking are used in the control of other natural behaviors. We compared the three synergies extracted from kicks with the synergies extracted from three other behaviors. We collected EMGs during 487 jumps, 1,409 swimming cycles and 297 walking cycles in the same three frogs. Unlike the kicking behavior, we found that jumping, swimming and walking muscle patterns were best described by four synergies. For each of the six pairs of behaviors, we compared the similarities between the best matching pairs of synergies extracted from two different behaviors with the similarities between the best matching pairs of random synergies (**Fig. 7**). We generated random synergies according to the amplitude distribution of the individual muscles in each behavior (Methods). We first compared the three synergies extracted from kicking (**Fig. 3**) with the synergies extracted from jumping, swimming and walking (**Fig. 7**, first row of plots). The third synergy extracted from kicking (W_3) has a high similarity with one of the synergies extracted from jumping (0.88) and one of the synergies in walking (0.95). Moreover, the first synergy in the kicking set (W_1) has a moderate similarity with one of the synergies in swimming (0.71). Of the six remaining comparisons between the synergies extracted from kicking and the synergies from other behaviors, in four cases, the similarity is higher than between random synergies. These comparisons indicate that there are significant similarities among the synergies extracted from kicking and from different natural behaviors and suggest that at least one kicking synergy is shared across tasks.

Further evidence for sharing of synergies across behaviors came from comparing the synergies extracted from jumping, swimming and walking (**Fig. 7**, second row of plots). A similarity above 0.73 was found for three out of four synergy comparisons in jumping versus swimming and in jumping versus walking. In the case of swimming versus walking, only two out of four pairs showed a similarity above 0.73. For the remaining four pairs with a similarity below 0.73, two showed a similarity higher than between random synergies. Taken together, these results suggest that a number of muscle synergies are shared in the control of different natural motor behaviors.

Discussion

We have shown that the variety of muscle patterns underlying the control of a natural behavior in an intact animal can be recon-

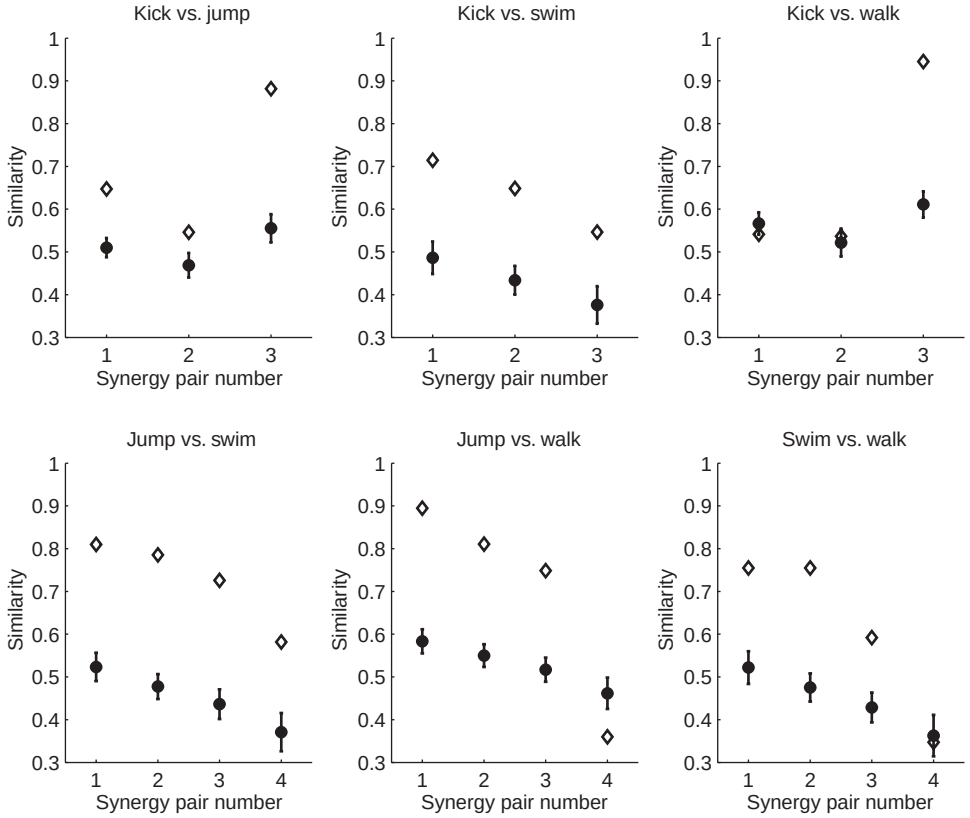

Fig. 7. Comparison among synergies extracted from kicking, jumping, swimming and walking. Each plot shows the values of the similarity (Methods) between the best matching pairs of synergies in each one of the six pairs of behaviors. The three plots in the first row show the similarities (open diamonds) between the three synergies extracted from kicking (W_1 to W_3 of **Fig. 3**) and three out of the four synergies extracted from jumping, swimming and walking, and the similarities between the best matching pairs of randomly generated synergies (filled circles, mean ± s.d.). The plots on the second row show the similarities (open diamonds) between the four best matching synergy pairs among jumping, swimming and walking, ordered according to their degree of similarity, contrasted to the similarities between the best matching pairs of randomly generated synergies (filled circles, mean ± s.d.).

structed as combinations of a small number of discrete elements. These elements, time-varying muscle synergies, capture the invariant spatio-temporal structure present in the patterns. That is, they are components shared among different patterns that each represent a specific activation level and time-course of a group of muscles. Because of this decomposition, we were able to describe the differences across the patterns observed during individual trials of kicking simply as differences in the amplitude scaling and time delaying of three time-varying synergies. We found that the level and time of recruitment of two of the three synergies were systematically modulated in relation to the movement kinematics. In particular, the amount of hip and knee extension was related to both the amplitude ratio and the timing difference of the two synergies. Finally, we found similarities among the three synergies extracted from kicking and the synergies extracted from three different behaviors.

Our decomposition method is novel because it extracts a set of time-varying generators that can be independently shifted in time. Other decomposition methods, either linear (PCA[14], ICA[15,16]) or with non-negative constraints[8,17], can extract a set of generators only in the spatial domain; that is, they can only represent synchronous muscle synergies. These methods can also extract time-varying synergies if samples at different times are treated as additional spatial dimensions, but these synergies will all have the same latency and cannot be shifted in time independently.

We have extracted a set of synergies whose combinations reconstruct the entire set of observed muscle patterns. A small number of components is sufficient to explain a large fraction of the variation in the observed data, indicating that the data lie in a low-dimensional space. This result represents a remarkable simplification in view of the high dimensionality of the space of all possible time-varying muscle patterns. One potential explanation for this observed low-dimensionality might be the existence of constraints on the muscle patterns deriving from the specific movements required by the task. However, we think that it is unlikely that the observed dimensionality reduction simply arises from task-dependent constraints. First, even for a simple behavior described by a single parameter (such as kick direction), the set of muscle patterns capable of generating the entire movement repertoire need not be embedded in a low-dimensional space. Given the redundancy of the musculoskeletal system, the same goal can be achieved by different movements, and the same movement can be generated by different muscle combinations, for example with different levels of co-contraction around a joint. Therefore, already the set of muscle patterns associated to a single value of the parameter describing the task could have high dimensionality. Second, in the same way that a curve in space may lie on a line, on a plane or in a volume, the set of muscle patterns associated with one task parameter, a one-dimensional manifold in the space of all possible muscle patterns, may be embedded in a subspace of any dimension up to the very high

dimension of the muscle pattern space. Thus, on theoretical grounds, task-dependent constraints do not ensure low-dimensionality of the muscle patterns *per se*. Third, if the low dimensionality resulted purely from task-dependent constraints, one would not expect to see many similarities between synergies across different tasks. We instead observed many similarities among the synergies extracted from different behaviors (**Fig. 7**). Thus, we believe that the observed low-dimensionality is a distinctive feature of a controller that is based on the combinations of a small number of discrete elements.

The structure of the extracted synergies and the modulation of their recruitment across different movements suggest that they may implement basic biomechanical functions. For example, in the first synergy (W_1 in **Fig. 3**), two hip extensor muscles (RI and SM) are highly activated, and this synergy is maximally recruited in kicks involving a hip extension. Each of the extracted synergies, however, shows a relatively complex spatiotemporal pattern of muscle activation. For example, an ankle extensor (GA) is recruited together with the hip extensors in the first synergy, and a delay is introduced between the activation of two knee extensors (VI and VE) in the second synergy (W_2 in **Fig. 3**). We speculate that the specific structure of these synergies might arise not only from the need to implement simple biomechanical functions, but also as the result of an optimization process aimed at increasing the range of movements and goals that could be achieved using a limited number of control elements. In the case of genetically specified behaviors, this optimization process might have taken place through evolution. Thus, time-varying synergies might provide the frog's motor system not just with a way to control a group of muscles as a unit, but also with those specific spatiotemporal muscle activations that may work as a basis and allow the control of a variety of movements by simple combination rules.

The data described here supports the hypothesis that the intact CNS simplifies the control of a large number of degrees of freedom by the combination of discrete elements. This hypothesis has been put forward in different forms by many investigators, but the strongest experimental evidence in its favor has come mainly from observations conducted in reduced preparations. Since Sherrington's proposal of reflex chaining[18] and Brown's idea of reciprocally inhibiting centers[19], many experimentalists have used spinalized or decerebrated animals to characterize pattern-generating[8,9,20–23] and force field– generating[5,6,24,25] systems that act as building blocks in the construction of movement. The use of reduced preparations, however, has in many cases made it difficult to relate these results to the generation of natural behaviors of intact animals. On the other hand, the study of intact animals and humans has been inconclusive with respect to the existence of discrete building blocks. In many of these studies, the existence of muscle synergies has been assessed by studying the amplitude correlations[26,27], cross-correlations[27,28] or tuning similarities[29,30] among muscles involved in different forms of a motor task. But pairwise correlations may be inconclusive if the muscles in a pair are shared by two synergies recruited simultaneously. Instead, the decomposition method used here, by distinguishing the contribution of different synergies to the activation of each muscle, can identify coherent components in the muscle patterns even when pairwise correlations are masked by the simultaneous recruitment of several synergies.

The control of limb trajectory depends on both the amplitude and the time of activation of the entire set of limb muscles. In primates, the recruitment amplitude and timing of several muscles depend systematically on the direction of reaching movements of the arm[31–33] or the direction of step tracking movements of the wrist[34]. Although these studies suggest the existence of simple rules for the generation of the commands needed to control the direction of movements, they also reveal the complexity of the spatiotemporal patterns of muscle activation beyond a simple 'triphasic' pattern. In the frog, our results indicate a comparable relationship between movement kinematics and synergy recruitment. Specifically, the observation of the similarity between the dependence on kinematic variables of magnitude ratio and onset-time difference of two extension synergies (**Fig. 6b** and **c**) is analogous to the observation reported in primates concerning the recruitment of agonist at the shoulder and elbow during reaching movements in a horizontal plane[32,35]. Thus the time-varying synergies model improves upon previous accounts based on single or pairs of muscles: not only does it describe the relationships between muscle recruitment and kinematic variables, but it also provides a quantitative framework to explain the complex relationship between amplitude and timing of the entire muscle pattern.

Bernstein argued that movements are complex objects in space and time that adapt their structure to solve an infinite number of motor problems[1]. Our results suggest that these complex objects are constructed by the nervous system as combinations of time-varying muscle synergies.

Methods

Electrode implantation. All procedures were approved by the Committee on Animal Care at MIT. Four adult bullfrogs (*Rana catesbeiana*) were studied. After the injection of 1 ml of tricaine (5%, *m*-aminobenzoic acid ethyl ester methanesulfonate, MS-222, Sigma) in the dorsal lymph sac, frogs were kept on ice during the procedure. We implanted bipolar electrodes in the following muscles (using previously established nomenclature[36]): rectus internus major (RI), adductor magnus (AD), semimembranosus (SM), vastus internus (VI), vastus externus (VE), rectus anterior (RA), peroneus (PE), gastrocnemius (GA), ventral head of semitendinosus (ST), sartorius (SA), biceps (or ilio-fibularis, BI), iliopsoas (IP) and tibialis anterior (TA). This set includes the majority of the muscles in the frog hindlimb. The sign of the most significant moment arms around hip, knee and ankle flexion-extension axes for each muscle[37,38] is indicated in **Fig. 3**. The wires were led subcutaneously to the back and, through a skin incision, connected to a multi-pin miniature connector using crimp contacts and shrink tubing for insulation. The connector was secured to the skin with tissue glue.

Data collection and analysis. Kicking, jumping and walking muscle patterns were collected from unrestrained frogs freely moving in a large cage. Swimming patterns were recorded in a specially designed tank. Kicking behavior was elicited by gently scratching the skin with a wooden tip or with fine forceps on a variety of locations on the frog's foot. EMGs were band-pass filtered (10 Hz to 1 kHz), amplified (gain 5,000) and digitized at 1 kHz. Movements were videotaped using a digital video camera (29.97 frames/s, Sony TRV-9).

For data analysis, we used custom software written in Matlab (MathWorks, Natick, Massachusetts). Using the video recordings, continuous EMG traces were parsed into segments associated with individual kicks, jumps, swimming cycles and walking cycles. EMGs were rectified, low-pass filtered (20 Hz cut-off using a FIR filter of length 50) and integrated over 10-ms intervals. The resulting samples were then normalized to the amplitude of the maximum sample.

Time-varying synergies model. We modeled the generation of muscle patterns as combinations of time-varying muscle synergies, that is, coordinated activations of a group of muscles with a specific time course for each muscle. To construct a particular muscle pattern, each synergy can be independently scaled in amplitude and shifted in time (**Fig. 1**). If we represent the activation of a set of D muscles as a time sequence of D dimensional vectors $\mathbf{m}(t)$, we can express it as combinations of N time-varying synergies $\{\mathbf{w}_i(t)\}_{i=1,..,N}$

$$\mathbf{m}(t) = \sum_{i=1}^{N} c_i \mathbf{w}_i (t - t_i) \tag{1}$$

where c_i is a non-negative scaling coefficient for the i-th synergy, and t_i is the synergy onset delay. Given a maximum duration for the synergies of T_{max} corresponding to J samples at discrete times τ_j (j=1,…,J), we can express the time-varying synergies using a set of N matrices, each made of D rows and J columns, whose columns $\{\mathbf{W}^i_j\}_{j=1,\ldots,J}$ are D dimensional vectors representing the muscle activation levels for the i^{th} synergy at the j^{th} time sample:

$$\mathbf{w}_i(\tau_j) = \begin{cases} 0 & \tau_j < 0 \\ \mathbf{W}^i_j & 0 \le \tau_j < \mathbf{T}_{max} \\ 0 & \tau_j \ge \mathbf{T}_{max} \end{cases} \tag{2}$$

Since muscle activation is a non-negative quantity, we also constrain the elements of $\mathbf{W}^i_j$ to be non-negative.

Our model does not explicitly incorporate sensory feedback signals in the generation of muscle patterns. Nonetheless, sensory information can still affect the motor output by modulating both scaling coefficients and onset delays.

Decomposition algorithm. We used a more efficient version of our decomposition algorithm[12] to extract a set of N time-varying synergies which minimizes the total squared reconstruction error on a set of S observed muscle patterns. This algorithm uses a multiplicative update rule[39] for the optimization of non-negative amplitude coefficients and synergy elements. To perform the matrix multiplications required by this algorithm, we rewrote equation (1) for the s^{th} pattern as

$$\mathrm{M}_s = \mathrm{W}\,\mathrm{H}_s \tag{3}$$

using the matrix M_s (with D rows and k_s columns) whose columns are the vectors $\mathbf{m}(t)$ from all the samples of the s^{th} muscle pattern; the matrix W (with D rows and $N \times J$ columns) whose columns are the vectors $\mathbf{W}^i_j$ (arranged so that the i^{th} block of adjacent J columns corresponds to the i^{th} synergy, that is, the matrix W_i); and the matrix H_s (with $N \times J$ rows and k_s columns), which has the function of scaling in amplitude and shifting in time the N synergies in the s^{th} pattern by matrix multiplication. This matrix is obtained from the amplitude and timing coefficients

$$\mathrm{H}_s = \sum_i c_{is}\, \Theta_i[t_{is}] \tag{4}$$

using a matrix $\Theta_i[\tau]$ whose product with W shifts the onset of the i^{th} synergy at the time τ_j (with $1 - J \le j < J_s$, J_s being the number of samples of the s^{th} muscle pattern) and truncates the synergy if partially shifted beyond the beginning or the end of the muscle pattern. For each delay τ_j, the only non-zero rows in $\Theta_i[\tau_j]$ are those relative to the i^{th} synergy, and they contain only ones along a diagonal starting at the $j + 1$ column and finishing at the column $j + J$. The element of the p^{th} row and q^{th} column of $\Theta_i[\tau_j]$ can be expressed using the Kroneker delta as:

$$\left[\Theta_i[\tau_j]\right]_{pq} = \delta\left[p - (i-1)\cdot J,\, q - j\right]. \tag{5}$$

Finally, for the entire set of S observed muscle patterns, we can write M = WH, where both M and H are obtained by adjoining the columns of the S matrices relative to each single pattern.

We used an iterative procedure to minimize the total reconstruction error:

$$E^2 = tr\left((\mathrm{M} - \mathrm{WH})^T (\mathrm{M} - \mathrm{WH})\right) \tag{6}$$

where $tr(\cdot)$ is the trace operator summing over the elements on the matrix diagonal, corresponding to the sum of squared residual for all the elements of the matrix M. First, we initialize synergies and coefficients to random positive values in the [0 1] interval. We then iterated the following steps:

For each observed pattern M_s, given the synergies W and the scaling coefficients c_{is}, we found the delays t_{is} using a nested matching procedure based on the maximization of the cross-correlation of the synergies with the data[12].

For each pattern, given the synergies and the delays, we updated the scaling coefficients using

$$c_{is} \leftarrow c_{is}\, \frac{tr(\mathrm{M}_s^T \mathrm{W}\, \Theta_i[t_{is}])}{tr(\mathrm{H}_s^T \mathrm{W}^T \mathrm{W}\, \Theta_i[t_{is}])}, \tag{7}$$

where the denominator and numerator of this expression correspond respectively to the positive term and the absolute value of the negative term in the expression for the gradient of E^2 with respect to c_{is}.

Given the delays and the scaling coefficients, we updated the synergies matrix using

$$\mathrm{W} \leftarrow \mathrm{W}\, \frac{\mathrm{M}\,\mathrm{H}^T}{\mathrm{W}\,\mathrm{H}\,\mathrm{H}^T}, \tag{8}$$

where the elements of the denominator and numerator correspond to the positive terms and the absolute value of the negative terms in the expression for the gradient of E^2 with respect to the elements of the matrix W.

To minimize the probability of finding a local minimum as the solution of the optimization, we repeated the procedure several times and selected the solution with the highest R^2. In general, we found that the difference in R^2 in different runs was very small, and the extracted synergies were very similar.

Cross-validation procedure. We used a cross-validation procedure[13] to select the number of synergies. As this number increases, additional synergies may start capturing the noise in the specific dataset (over-fitting) more that the underlying structure of the data. To avoid this problem, we determined the model order with the best generalization performance—the best reconstruction of the data not used to fit the model. We first randomly partitioned the entire dataset in five sets of approximately equal size. We then extracted a set of synergies from each one of the five combinations of four of the five groups. Finally, we evaluated the reconstruction error (validation error) for those synergies on the remaining group (test set). We repeated this procedure for sets ranging from one to ten synergies and, for each number, we computed the mean validation R^2 over the five validation sets.

Similarity between synergies. We quantified the similarity between two time-varying synergies using the maximum of their normalized scalar products over all possible delays. In detail, given two normalized synergies $\mathbf{w}_1$ and $\mathbf{w}_2$ (each D rows and J columns), for each possible delay j of the second synergy, $j \in [1{-}J, J)$, we first build a vector $\mathbf{v}_1^j$ of $D \times J$ elements by first translating by j and truncating at the edges each one of the D rows of $\mathbf{w}_1$, and then rearranging in a single column the D rows of $\mathbf{w}_1$. We then build a vector $\mathbf{v}_2$ obtained by rearranging on a single column the D rows of $\mathbf{w}_2$. Finally, we define the similarity S as the maximum of the scalar products.

$$S = \max_{j \in [1-J, J)} (\mathbf{v}_2^{\mathrm{T}} \bullet \mathbf{v}_1^j) \tag{9}$$

Therefore, given this definition, the similarity for non-negative synergies ranges from 0 to 1.

We compared the synergies in two sets by computing the similarities between the best matching pairs. We started by selecting the pair with

the highest similarity, and then the synergies in that pair were removed from their sets. We then computed the similarities between the remaining synergies and selected the next best matching pair. We repeated this procedure until all synergies in the smallest set had been matched.

Random synergies. We used random synergies to assess the specificity of the extracted synergies in reconstructing the observed pattern and to evaluate the significance of the similarity measure introduced above. We generated random synergies of the same length than the extracted synergies by randomly choosing their elements from the observed amplitude distribution of each muscle. We then low-pass filtered the random synergies (20 Hz cut-off) to generate synergies with a smoothness similar to the data and the extracted synergies. We fitted the random synergies to the data by selecting amplitude and timing coefficients with the same algorithm used for synergy extraction, with the exception of the synergy update step. We estimated the significance of the similarity between the best matching pairs of synergies in two different synergy sets by generating the same number of random synergies as in those sets and by selecting the best matching pairs of random synergies with the same procedure used for the extracted synergies (see above). We computed the mean and the standard deviation of the similarity between the best matching pairs of random synergies by repeating the random generation 100 times.

Kick kinematics. We extracted joint kinematics from digitized video frames. Assuming a planar motion of the limb, we computed the time sequence of joint angles from markers placed on individual fields (59.64 Hz). For each kick, we computed a vector in the hip–knee plane measuring the displacement between the initial hip–knee coordinates and the coordinates at the maximum extension, that is, at the maximum distance in the hip-knee plane from the initial position. To quantify the relationship between recruitment of the first two extracted synergies and the displacement vector direction, we first removed the kicks with an activation magnitude for the first (c_1) or second (c_2) synergy below the 10th percentile of the distribution of each coefficient. We then computed, for the remaining kicks ($n = 191$), the average logarithm of the ratio of c_1 over c_2 (**Fig. 6b**) and the average synergy onset delay difference ($t_2 - t_1$, **Fig. 6c**) over ten bins with different displacement vector directions. The bins were defined using the angle between the displacement vector direction and the direction of a pure hip extension. Each bin included the kicks between two successive deciles of the angle distribution.

Acknowledgments

We thank M. Tresch for many helpful discussions and suggestions, S. Mussa-Ivaldi, M. Mezzetti, D. Grodner, A. Rebek and C. Gulledge for comments on the manuscript, S. Dalai and J. O'Vari for helping with the experiments and the analysis of kinematic data, and M. Cantor for constant and irreplaceable support. Supported by NIH-NINDS NS09343.

Competing interests statement

The authors declare that they have no competing financial interests.

RECEIVED 15 NOVEMBER 2002; ACCEPTED 8 JANUARY 2003

1. Bernstein, N. *The Co-ordination and Regulation of Movement* (Pergamon, Oxford, 1967).
2. Hogan, N. Planning and execution of multijoint movements. *Can. J. Physiol. Pharmacol.* **66**, 508–517 (1988).
3. Sherrington, C.S. *The Integrative Action of the Nervous System* (Univeristy Press, Cambridge, England, 1948).
4. Grillner, S. Control of locomotion in bipeds, tetrapods and fish. in *Handbook of Physiology: Sect I. The Nervous System* (ed. Brooks, V.B.) 1179–1236 (American Physiological Society, Bethesda, Maryland, 1981).
5. Bizzi, E., Mussa-Ivaldi, F.A. & Giszter, S.F. Computations underlying the execution of movement: a biological perspective. *Science* **253**, 287–291 (1991).
6. Giszter, S.F., Mussa-Ivaldi, F.A. & Bizzi, E. Convergent force fields organized in the frog's spinal cord. *J. Neurosci.* **13**, 467–491 (1993).
7. Mussa-Ivaldi, F.A., Giszter, S.F. & Bizzi, E. Linear combinations of primitives in vertebrate motor control. *Proc. Natl. Acad. Sci. USA* **91**, 7534–7538 (1994).
8. Tresch, M.C., Saltiel, P. & Bizzi, E. The construction of movement by the spinal cord. *Nat. Neurosci.* **2**, 162–167 (1999).
9. Saltiel, P., Wyler-Duda, K., D'Avella, A., Tresch, M.C. & Bizzi, E. Muscle synergies encoded within the spinal cord: evidence from focal intraspinal NMDA iontophoresis in the frog. *J. Neurophysiol.* **85**, 605–619 (2001).
10. Lee, W.A. Neuromotor synergies as a basis for coordinated intentional action. *J. Mot. Behav.* **16**, 135–170 (1984).
11. Macpherson, J.M. How flexible are muscle synergies? in *Motor Control: Concepts and Issues* (eds. Humphrey, D.R. & Freund, H.-J.) 33–47 (Wiley, Chichester, UK, 1991).
12. d'Avella, A. & Tresch, M.C. Modularity in the motor system: decomposition of muscle patterns as combinations of time-varying synergies. in *Advances in Neural Information Processing Systems 14* (eds. Dietterich, T.G., Becker, S. & Ghahramani, Z.) 141–148 (MIT Press, Massachusetts, 2002).
13. Bishop, C. *Neural Networks for Pattern Recognition* (Claredon, Oxford, UK, 1995).
14. Mardia, K.V., Kent, J.T. & Bibby, J.M. *Multivariate Analysis* (Academic, London; New York, 1979).
15. Bell, A.J. & Sejnowski, T.J. An information-maximization approach to blind separation and blind deconvolution. *Neural Comput.* **7**, 1129–1159 (1995).
16. Makeig, S., Jung, T.P., Bell, A.J., Ghahremani, D. & Sejnowski, T.J. Blind separation of auditory event-related brain responses into independent components. *Proc. Natl. Acad. Sci. USA* **94**, 10979–10984 (1997).
17. Lee, D.D. & Seung, H.S. Learning the parts of objects by non-negative matrix factorization. *Nature* **401**, 788–791 (1999).
18. Sherrington, C.S. Flexion-reflex of the limb, crossed extension reflex and reflex stepping and standing. *J. Physiol. (Lond.)* **40**, 28–121 (1910).
19. Brown, T.G. The intrinsic factors in the act of progression in the mammal. *Proc. R. Soc. Lond. B Biol. Sci.* **84**, 308–319 (1911).
20. Grillner, S. & Zangger, P. On the central generation of locomotion in the low spinal cat. *Exp. Brain Res.* **34**, 241–261 (1979).
21. Rossignol, S. & Dubuc, R. Spinal pattern generation. *Curr. Opin. Neurobiol.* **4**, 894–902 (1994).
22. Stein, P.S., McCullough, M.L. & Currie, S.N. Spinal motor patterns in the turtle. *Ann. NY Acad. Sci.* **860**, 142–154 (1998).
23. Cheng, J. *et al.* Identification, localization, and modulation of neural networks for walking in the mudpuppy (*Necturus maculatus*) spinal cord. *J. Neurosci.* **18**, 4295–4304 (1998).
24. Saltiel, P., Tresch, M.C. & Bizzi, E. Spinal cord modular organization and rhythm generation: an NMDA iontophoretic study in the frog. *J. Neurophysiol.* **80**, 2323–2339 (1998).
25. Kargo, W.J. & Giszter, S.F. Rapid correction of aimed movements by summation of force-field primitives. *J. Neurosci.* **20**, 409–426 (2000).
26. Buchanan, T.S., Almdale, D.P.J., Lewis, J.L. & Rymer, W.Z. Characteristics of synergic relations during isometric contractions of human elbow muscles. *J. Neurophysiol.* **56**, 1225–1241 (1986).
27. Maier, M.A. & Hepp-Reymond, M.C. EMG activation patterns during force production in precision grip. II. Muscular synergies in the spatial and temporal domain. *Exp. Brain Res.* **103**, 123–136 (1995).
28. Soechting, J.F. & Lacquaniti, F. An assessment of the existence of muscle synergies during load perturbations and intentional movements of the human arm. *Exp. Brain Res.* **74**, 535–548 (1989).
29. Macpherson, J.M. Strategies that simplify the control of quadrupedal stance. II. Electromyographic activity. *J. Neurophysiol.* **60**, 218–231 (1988).
30. Henry, S.M., Fung, J. & Horak, F.B. EMG responses to maintain stance during multidirectional surface translations. *J. Neurophysiol.* **80**, 1939–1950 (1998).
31. Wadman, W., Dernier van der Gon, J.J. & Derksen, R.J.A. Muscle activation patterns for fast goal-directed arm movements. *J. Hum. Mov. Stud.* **6**, 19–37 (1980).
32. Karst, G.M. & Hasan, Z. Timing and magnitude of electromyographic activity for two-joint arm movements in different directions. *J. Neurophysiol.* **66**, 1594–1604 (1991).
33. Flanders, M., Pellegrini, J.J. & Soechting, J.F. Spatial/temporal characteristics of a motor pattern for reaching. *J. Neurophysiol.* **71**, 811–813 (1994).
34. Hoffman, D.S. & Strick, P.L. Step-tracking movements of the wrist. IV. Muscle activity associated with movements in different directions. *J. Neurophysiol.* **81**, 319–333 (1999).
35. Scott, S.H. Comparison of onset time and magnitude of activity for proximal arm muscles and motor cortical cells before reaching movements. *J. Neurophysiol.* **77**, 1016–1022 (1997).
36. Ecker, A. *The Anatomy of the Frog* (Claredon, Oxford, 1889).
37. Lombard, W.P. & Abbott, F.M. The mechanical effect produced by the contraction of individual muscles of the thigh of the frog. *Am. J. Physiol.* **20**, 1–60 (1907).
38. Kargo, W.J. & Rome, L.C. Functional morphology of proximal hindlimb muscles in the frog *Rana pipiens*. *J. Exp. Biol.* **205**, 1987–2004 (2002).
39. Lee, D.D. & Seung, H.S. Algorithms for non-negative matrix factorization. in *Advances in Neural Information Processing Systems* Vol. 13 (eds. Leen, T.K., Dietterich, T.G. & Tresp, V.) 556–562 (MIT Press, Massachusetts, 2001).